materials

MDPI

Article

Impact of Diverse Parameters on the Physicochemical Characteristics of Green-Synthesized Zinc Oxide–Copper Oxide Nanocomposites Derived from an Aqueous Extract of *Garcinia mangostana* L. Leaf

Yu Bin Chan [1], Mohammod Aminuzzaman [1,2,*], Lai-Hock Tey [1,*], Yip Foo Win [1], Akira Watanabe [3], Sinouvassane Djearamame [4] and Md. Akhtaruzzaman [5]

[1] Department of Chemical Science, Faculty of Science, Universiti Tunku Abdul Rahman (UTAR), Kampar Campus, Jalan Universiti, Bandar Barat, Kampar 31900, Malaysia; yubinchan1221@gmail.com (Y.B.C.); yipfw@utar.edu.my (Y.F.W.)
[2] Centre for Photonics and Advanced Materials Research (CPAMR), Universiti Tunku Abdul Rahman (UTAR), Sungai Long Campus, Jalan Sungai Long, Bandar Sungai Long, Kajang 43000, Malaysia
[3] Institute of Multidisciplinary Research for Advanced Materials (IMRAM), Tohoku University, Sendai 980-8577, Japan; akira.watanabe.c6@tohoku.ac.jp
[4] Department of Biomedical Science, Faculty of Science, Universiti Tunku Abdul Rahman (UTAR), Kampar Campus, Jalan Universiti, Bandar Barat, Kampar 31900, Malaysia; sinouvassane@utar.edu.my
[5] Solar Energy Research Institute (SERI), Universiti Kebangsanan Malaysia (UKM), Bangi 43600, Malaysia; akhtar@ukm.edu.my
* Correspondence: mohammoda@utar.edu.my (M.A.); teylh@utar.edu.my (L.-H.T.)

Abstract: Compared to conventional metal oxide nanoparticles, metal oxide nanocomposites have demonstrated significantly enhanced efficiency in various applications. In this study, we aimed to synthesize zinc oxide–copper oxide nanocomposites (ZnO-CuO NCs) using a green synthesis approach. The synthesis involved mixing 4 g of $Zn(NO_3)_2{\cdot}6H_2O$ with different concentrations of mangosteen (*G. mangostana*) leaf extract (0.02, 0.03, 0.04 and 0.05 g/mL) and 2 or 4 g of $Cu(NO_3)_2{\cdot}3H_2O$, followed by calcination at temperatures of 300, 400 and 500 °C. The synthesized ZnO-CuO NCs were characterized using various techniques, including a UV-Visible spectrometer (UV-Vis), photoluminescence (PL) spectroscopy, Fourier Transform Infrared (FTIR) spectroscopy, X-ray powder diffraction (XRD) analysis and Field Emission Scanning Electron Microscope (FE-SEM) with an Energy Dispersive X-ray (EDX) analyzer. Based on the results of this study, the optical, structural and morphological properties of ZnO-CuO NCs were found to be influenced by the concentration of the mangosteen leaf extract, the calcination temperature and the amount of $Cu(NO_3)_2{\cdot}3H_2O$ used. Among the tested conditions, ZnO-CuO NCs derived from 0.05 g/mL of mangosteen leaf extract, 4 g of $Zn(NO_3)_2{\cdot}6H_2O$ and 2 g of $Cu(NO_3)_2{\cdot}3H_2O$, calcinated at 500 °C exhibited the following characteristics: the lowest energy bandgap (2.57 eV), well-defined Zn-O and Cu-O bands, the smallest particle size of 39.10 nm with highest surface area-to-volume ratio and crystalline size of 18.17 nm. In conclusion, we successfully synthesized ZnO-CuO NCs using a green synthesis approach with mangosteen leaf extract. The properties of the nanocomposites were significantly influenced by the concentration of the plant extract, the calcination temperature and the amount of precursor used. These findings provide valuable insights for researchers seeking innovative methods for the production and utilization of nanocomposite materials.

Keywords: *Garcinia mangostana* L.; green product; green synthesis; nanocomposites; zinc oxide-copper oxide

check for updates

Citation: Chan, Y.B.; Aminuzzaman, M.; Tey, L.-H.; Win, Y.F.; Watanabe, A.; Djearamame, S.; Akhtaruzzaman, M. Impact of Diverse Parameters on the Physicochemical Characteristics of Green-Synthesized Zinc Oxide–Copper Oxide Nanocomposites Derived from an Aqueous Extract of *Garcinia mangostana* L. Leaf. *Materials* **2023**, *16*, 5421. https://doi.org/10.3390/ma16155421

Academic Editor: Slavko Bernik

Received: 27 May 2023
Revised: 6 July 2023
Accepted: 21 July 2023
Published: 2 August 2023

Copyright: © 2023 by the authors. Licensee MDPI, Basel, Switzerland. This article is an open access article distributed under the terms and conditions of the Creative Commons Attribution (CC BY) license (https://creativecommons.org/licenses/by/4.0/).

1. Introduction

Compared to individual semiconductor metal oxide nanoparticles (NPs), such as zinc oxide (ZnO), copper oxide (CuO), nickel oxide (NiO), etc., the mixing of these NPs

has gained significant attention due to their excellent application in sensor, electrical and electronic products. Mixing semiconductor metal oxides allows for control over their structural, morphological and surface properties, making them important in various practical applications [1]. Among the *p-n* type mixed semiconductors, ZnO-CuO nanocomposites (NCs) garnered considerable interest from researchers. Copper is preferred to combine with ZnO due to its ability to easily overlap *d*-electrons with a valence bond of ZnO [2]. This results in enhanced surface area, smaller particle size and the formation of ZnO-CuO heterojunctions, which strengthen the optical and electronic properties [2,3]. Consequently, ZnO-CuO NCs find application in environmental remediation, photo-catalysis, fuel cell, solar cell, antibacterial, UV protection and optoelectronics devices [1,4–6]. For example, the effectiveness in degrading methylene blue was higher by using ZnO-CuO NCs (98%) compared to ZnO (81%) [5].

Green synthesis of nanomaterial offers a simpler, more cost-effective, eco-friendly alternative with lower energy consumption compared to conventional methods [7–12]. Generally, various parts of plants, including flowers, leaves, stems, roots and seeds, are utilized in the green synthesizing of nanomaterials [13–15]. During the green synthesis process, phytochemicals present in plants, such as phenols, aldehydes, ketones, carboxylic acids, nitrogenous compounds, flavonoids, alkaloids, terpenoids, tannins and pigments, accumulate and later interact with metals to cap, stabilize and reduce to NPs [9,16,17]. However, achieving the desired morphology and shape remains a challenge in the green synthesis of NPs and NCs. As a result, extensive research has been conducted to optimize the synthesis conditions, including plant extract concentration, temperature and precursor concentration, to synthesize NPs and NCs with desired structural, morphological and optical properties [18,19].

While aqueous extract from *Aloe barbadansis* leaf [3], *Calotropis gigantea* leaf [4], *Theobroma cacao* seed bark [6], *Dovyalis caffra* leaf [20], *Verbascum sinaiticum* Benth [21], *Sambucus nigra* L. shoot [22], *Alchornea cordifolio* leaf [23] and *Calotropis gigamtae* leaf [24] has been utilized for synthesizing ZnO-CuO NCs. The use of *Garcinia mangostana* L., commonly known as mangosteen, in synthesizing ZnO-CuO NCs has not been explored. Mangosteen is a seasonal fruit in the *Clusiacae* family and is commonly found in tropical countries [25–29]. It contains numerous phytochemicals, such as xanthones, flavonoids and terpene [30–33], which have the potential to form stable colloidal nanomaterials.

In this study, we synthesized ZnO-CuO NCs using a mangosteen leaf aqueous extract in a green, fast and simple manner. The mangosteen leaf aqueous extract-mediated ZnO-CuO NCs were optimized by varying the concentration of the mangosteen leaf aqueous extract (0.02, 0.03, 0.04 and 0.05 g/mL), calcination temperatures (300, 400 and 500 °C) and the amount of $Cu(NO_3)_2{\cdot}3H_2O$ (2.0 and 4.0 g). In this paper, we investigated the effects of these parameters (plant concentration, calcination temperature and precursor weight) on the optical, structural and morphological properties of the mangosteen leaf aqueous extract-mediated ZnO-CuO NCs.

2. Materials and Methods

2.1. Materials

The mangosteen leaves were collected from a neighborhood in Kampar, Malaysia. Zinc nitrate hexahydrate, $Zn(NO_3)_2{\cdot}6H_2O$, was purchased from HiMedia Laboratories Pvt. Ltd. (Nashik, India), and copper nitrate trihydrate, $Cu(NO_3)_2{\cdot}3H_2O$ was purchased from HmbG (Hamburg, Germany). Both chemicals were used without further purification. All glassware was washed with deionized water and dried in an oven before use.

2.2. Characterization

The selection of optimized parameters in green synthesizing ZnO-CuO NCs was based on their structural, morphological and optical properties. The absorption spectra were recorded by a UV-Visible (UV-Vis) spectrophotometer (Thermo Scientific GENESYS 10S, Waltham, MA, USA). The recombination of electron-hole pairs (e^-/h^+) of the synthesized

samples was investigated using photo luminance (PL) spectroscopy (Perkin Elmer LS 55 Fluorescence Spectrometer, Waltham, MA, USA) with an excitation wavelength of 350 nm in the range of 350 to 600 nm. The Fourier Transform Infrared (FTIR) spectroscopy study was carried out at room temperature in the range of 4000 to 400 cm^{-1} with a resolution of 4 cm^{-1} by using KBr pellets in a Perkin Elmer RX1 spectrophotometer. X-ray powder diffraction (XRD) patterns were taken in the reflection mode with Cu Kα (λ = 1.5406 Å) radiation in the 2θ range of 10° to 80° by using a Shimadzu XRD 6000 X-ray diffractometer with continuous scanning which was operated at 40 kV/30 mA and 0.02 min^{-1}. The morphological, microstructural and elemental compositional of all synthesized samples was determined using a Field Emission Scanning Electron Microscope (FE-SEM) (JEOL JSM-6710F, Tokyo, Japan) with Energy Dispersive X-ray (EDX) analyzer (X-max, 150 Oxford Instruments, Abingdon-*on*-Thames, UK).

2.3. Preparation of Mangosteen Leaf Aqueous Extract

The freshly plucked mangosteen leaves were washed with tap water to remove dust and dried in an oven at 50 °C for 48 h and further dried in a vacuum oven at 60 °C for 8 h. Then, the leaves were ground into a fine powder by using a grinder. Then, 5 g of leaf powder was added to 100 mL of deionized water and heated with stirring at 70–80 °C for 20 min to obtain 0.05 g/mL of leaf aqueous extract. Upon cooling, the leaf aqueous extract was vacuum filtrated, and a reddish-brown filtrate was collected and immediately used for ZnO-CuO NCs synthesis.

2.4. Synthesis of ZnO-CuO NCs

With minor modification from Chan et al. [34], the synthesis of ZnO-CuO NCs using mangosteen leaf aqueous extract was performed. The reaction parameters, which included mangosteen leaf aqueous extract concentration, calcination temperature and weight of $Cu(NO_3)_2{\cdot}3H_2O$ added, were optimized.

2.4.1. Leaf Aqueous Extract Optimization

The 50 mL of mangosteen leaf aqueous extract (0.02, 0.03, 0.04 and 0.05 g/mL) was mixed separately with 4.0 g of $Zn(NO_3)_2{\cdot}6H_2O$ and 2 g of $Cu(NO_3)_2{\cdot}3H_2O$. Immediately, a greenish-brown solution formed. The solution was heated at 70–80 °C with constant stirring until the formation of a brown paste. The paste was then cooled to room temperature and calcinated at 500 °C for 2 h using the Muffle furnace to obtain a fine black-blue ZnO-CuO powder.

2.4.2. Calcination Temperature Optimization

After the selection of the optimized mangosteen leaf aqueous extract concentration at 0.05 g/mL, the synthesis of ZnO-CuO NCs was repeated using 4 g of $Zn(NO_3)_2{\cdot}6H_2O$ and 2 g of $Cu(NO_3)_2{\cdot}3H_2O$. The cooled brown paste was calcinated at 300, 400 and 500 °C for 2 h to have more energy savings during the ZnO-CuO NCs synthesis.

2.4.3. Precursor Optimization

After the selection of the optimized mangosteen leaf aqueous extract concentration at 0.05 g/mL and calcination temperature at 500 °C, the synthesis steps were repeated using 4 g of $Zn(NO_3)_2{\cdot}6H_2O$ with different weights of $Cu(NO_3)_2{\cdot}3H_2O$ (2 and 4 g). Until the formation of brown paste. It was then calcinated at 500 °C for 2 h.

3. Results

3.1. UV-Vis Spectroscopy Analysis

Figure 1 shows the UV-Vis spectra of the mangosteen leaf aqueous extract, $Cu(NO_3)_2{\cdot}3H_2O$, $Zn(NO_3)_2{\cdot}6H_2O$ and mangosteen leaf aqueous extract-mediated ZnO-CuO NCs with their energy bandgap. The absorption peak position had no significant changes in ZnO-CuO NCs synthesized at different controlled parameters. The mangosteen leaf aqueous extract

absorption peak was located at 479 cm^{-1}, while for $Cu(NO_3)_2 \cdot 3H_2O$ and $Zn(NO_3)_2 \cdot 6H_2O$, it was located at 295 and 305 cm^{-1}, respectively. On the other hand, the ZnO-CuO NCs absorption peak was located at 369–375 cm^{-1}.

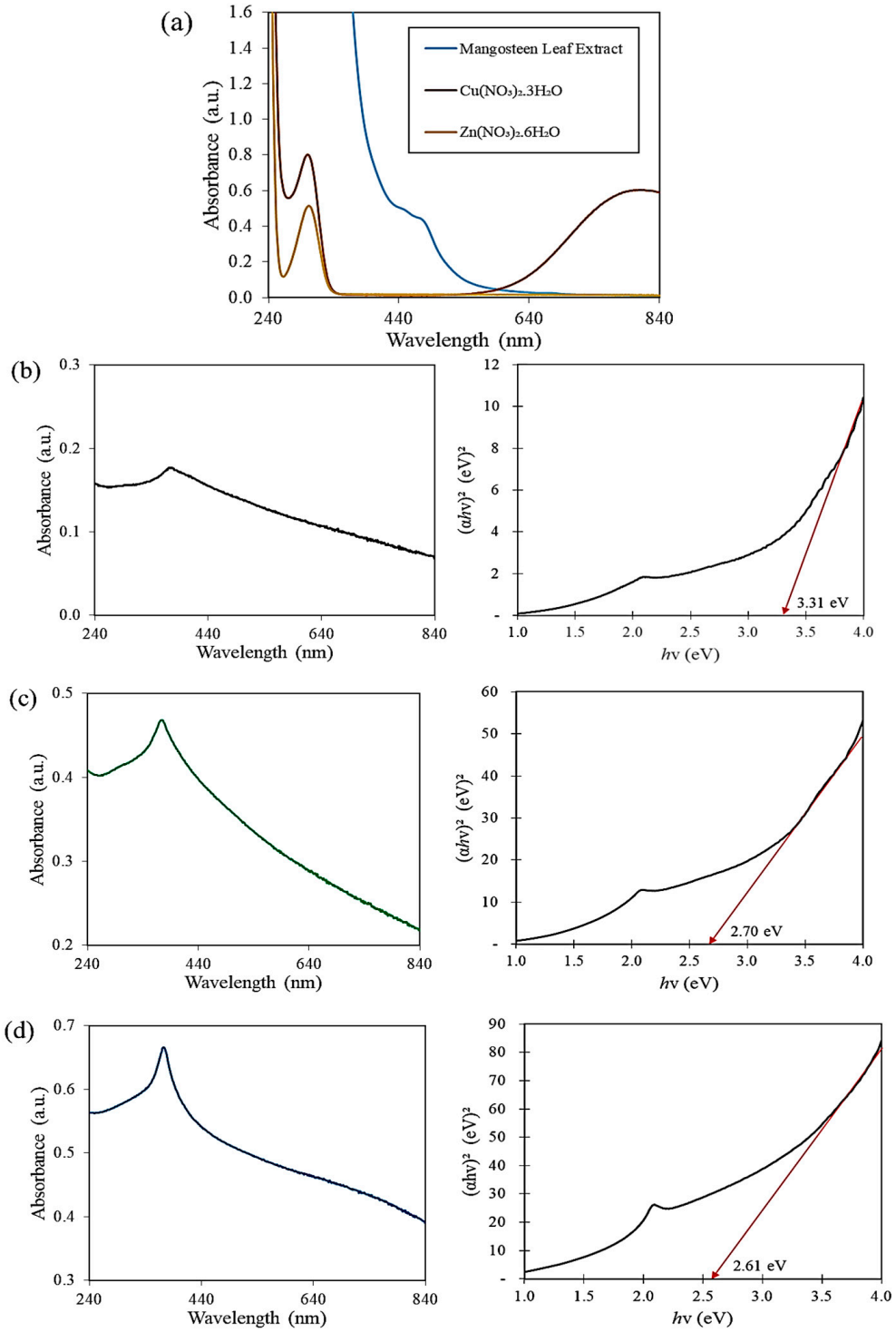

Figure 1. *Cont.*

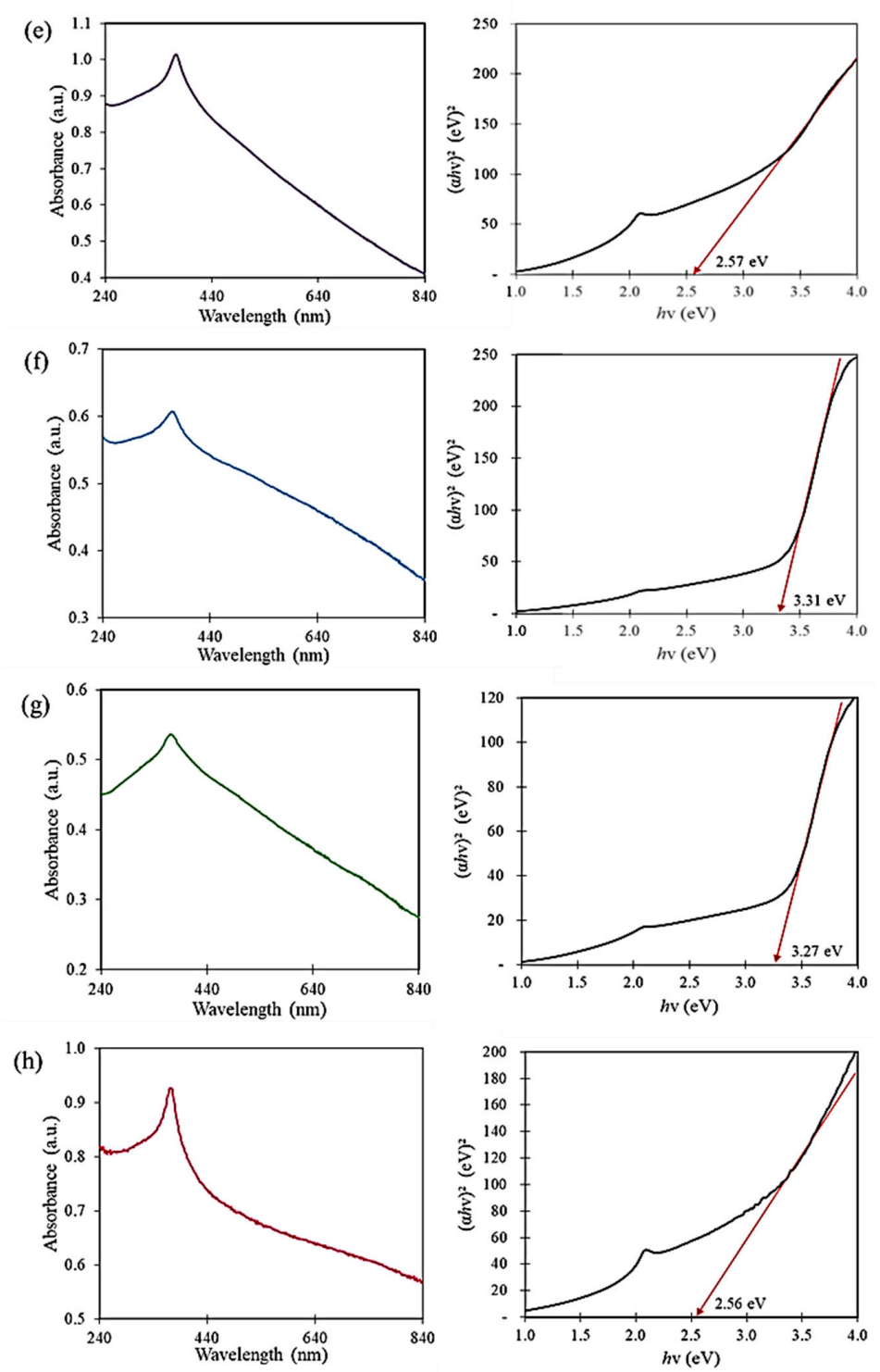

Figure 1. UV-Vis spectra (**left**) and energy bandgap (**right**) of (**a**) mangosteen leaf aqueous extract and green-synthesized ZnO-CuO NCs using (**b**) 0.02 g/mL, (**c**) 0.03 g/mL, (**d**) 0.04 g/mL and (**e**) 0.05 g/mL of mangosteen leaf extract; calcinated at (**f**) 300 °C and (**g**) 400 °C, respectively, by using 2 g of $Cu(NO_3)_2 \cdot 3H_2O$. Meanwhile, (**h**) is the UV-Vis spectrum (left) and energy bandgap (right) of 4 g of $Cu(NO_3)_2 \cdot 3H_2O$ calcinated at 500 °C by using 0.05 g/mL of mangosteen leaf aqueous extract.

The energy bandgap of the mangosteen leaf aqueous extract-mediated ZnO-CuO NCs at different synthesizing conditions is tabulated in Table 1. The energy band gap of

the ZnO-CuO NPs was expressed in eV and calculated using a Tauc-plot approach using Equation (1).

$$\alpha hv = A\left(hv - E_g\right)^n \quad (1)$$

where h is Plank's constant (6.626×10^{-34} Js), n is the exponential factor for electronic transition ($n = \frac{1}{2}$ for the indirect band, $n = 2$ for the direct band) and α is the absorption coefficient. The energy bandgap showed no significant difference when using 2 g (2.57 eV) and 4 g (2.56 eV) of $Cu(NO_3)_2{\cdot}3H_2O$ in synthesizing ZnO-CuO NCs. In contrast, a plant aqueous extract concentration-dependent and calcination temperature-dependent shifts were observed as the energy bandgap decreased from 3.31 eV to 2.57 eV and higher leaf aqueous extract concentrations and calcination temperatures were applied.

Table 1. Energy bandgap of green-synthesized ZnO-CuO NCs at different synthesizing condition parameters.

Mangosteen Leaf Aqueous Extract Concentration (g/mL)	Calcination Temperature (°C)	Weight of $Zn(NO_3)_2{\cdot}6H_2O$ (g)	Weight of $Cu(NO_3)_2{\cdot}3H_2O$ (g)	Energy Bandgap (eV)
0.02	500	4.0	2.0	3.31
0.03	500	4.0	2.0	2.70
0.04	500	4.0	2.0	2.61
0.05	500	4.0	2.0	2.57
0.05	300	4.0	2.0	3.31
0.05	400	4.0	2.0	3.27
0.05	500	4.0	4.0	2.56

3.2. FTIR Spectroscopy Analysis

The FTIR spectra interpretation of mangosteen leaf aqueous extract-mediated ZnO-CuO NCs at different controlled parameters is shown in Table 2, and their FTIR spectra are shown in Figure 2. The 3401–3436 cm^{-1} and 1629–1636 cm^{-1} bands corresponded to v(O-H) and v(C=O) or v(C=C). Moreover, 1384 cm^{-1} and 1099–1114 cm^{-1} bands were assigned to v(C-C aromatic) and v(C-O). The bond vibration of CuO and ZnO was indicated by the bands at 649–674 cm^{-1} and 447–524 cm^{-1}, respectively.

Table 2. Interpretation of FTIR spectra of green-synthesized ZnO-CuO NCs at different synthesizing condition parameters with the data presented in cm^{-1}.

Functional Groups	Parameters								
	Mangosteen Leaf Aqueous Extract Concentration (g/mL)				Calcination Temperature (°C)			Weight of $Cu(NO_3)_2{\cdot}3H_2O$ (g)	
	0.02	0.03	0.04	0.05 *	300	400	500 *	2 *	4
v(O-H)	3429	3435	3435	3435	3436	3435	3435	3435	3401
v(C=O), v(C=C)	1629	1636	1636	1636	1633	1635	1636	1636	1635
v(C-C aromatic)	1384	1384	1384	1384	1384	1384	1384	1384	1384
v(C-O)	1114	1108	1108	1108	1102	1099	1108	1108	1106
v(Cu-O)	674	660	649	651	657	657	651	651	672
v(Zn-O)	447	455	485	486	502	498	486	486	524

* The ZnO-CuO NCs were green-synthesized in the same conditions.

The v(C-C aromatic) and v(C=O) or v(C=C) intensities increased when higher concentrations of mangosteen leaf aqueous extract were used. On the other hand, v(C-C aromatic) and v(C=O) or v(C=C) intensities decreased, while v(Cu-O) intensity increased at elevated calcination temperatures. Additionally, the bands, which included v(C-C aromatic), v(C=O) or v(C=C), v(C-O) and v(Cu-O) intensities improved when more $Cu(NO_3)_2{\cdot}3H_2O$ was added.

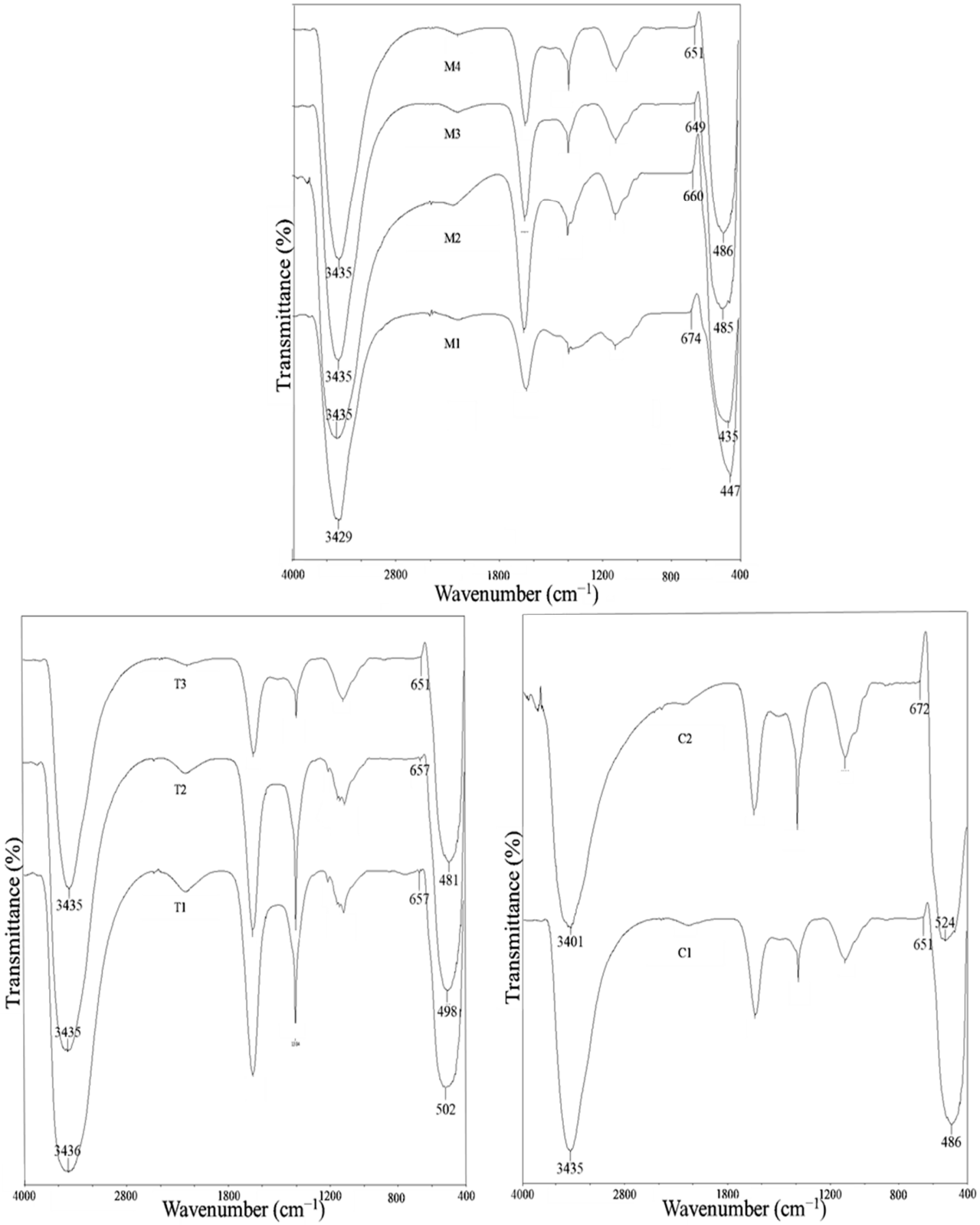

Figure 2. FTIR spectra of green-synthesized ZnO-CuO NCs at different controlled parameters: mangosteen leaf aqueous extract concentration (M1 = 0.02 g/mL, M2 = 0.03 g/mL, M3 = 0.04 g/mL and M4 = 0.05 g/mL), calcination temperature (T1 = 300 °C, T2 = 400 °C and T3 = 500 °C) and weight of $Cu(NO_3)_2 \cdot 3H_2O$ added (C1 = 2 g and C2 = 4 g), respectively.

3.3. PL Spectroscopy Analysis

The potential recombination of the photo-generated electron-hole (e^-/h^+) pairs of the mangosteen leaf aqueous extract-mediated ZnO-CuO NCs and the occurrence of their electronic transfer in NCs were determined by using PL spectroscopy (Figure 3). Overall, the ZnO-CuO NCs emission peaked in the violet region (390–405 nm). From Figure 3, it can be observed that the PL intensity was more affected by calcination temperature as high temperature-calcinated ZnO-CuO NCs had lower charge carrier separation compared to lower temperature samples.

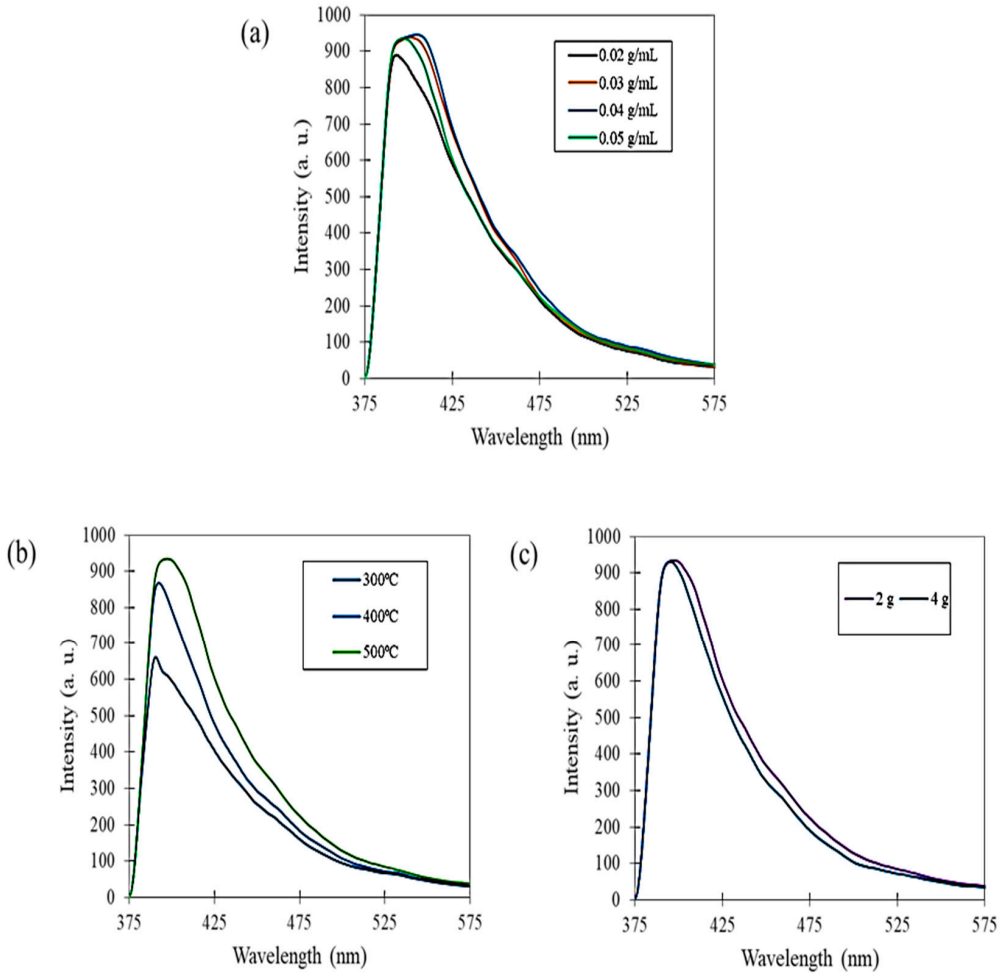

Figure 3. PL spectra of green-synthesized ZnO-CuO NCs under different parameters: (**a**) mangosteen leaf aqueous extract concentration, (**b**) calcination temperature and (**c**) weight of $Cu(NO_3)_2{\cdot}3H_2O$ added, respectively.

3.4. XRD Spectroscopy Analysis

The mangosteen leaf aqueous extract-mediated ZnO-CuO NCs with the reference card number ICDD 01-081-9217 were in a hexagonal-wurtzite phase, a = 3.2459 Å and c = 5.1975 Å, with space group *P*63*mc*. All peaks were very sharp and intense, indicating the samples were of a crystalline nature. ZnO-CuO NCs had diffraction peaks at 2θ values of 31.74, 34.41, 36.22, 47.57, 56.58, 62.90 and 69.03°, matched with the ZnO phase, indexed as (1 0 0), (0 0 2), (1 0 1), (1 0 2), (1 1 0), (1 0 3) and (2 0 1), respectively. Meanwhile, those 2θ values of 32.60, 35.58, 38.80, 48.59, 61.57, 66.30 and 68.01° matched with CuO phase were indexed as (−1 1 0), (0 0 2), (1 1 1), (−2 0 2), (−1 1 3), (0 2 2) and (−2 2 0), respectively. On the other hand, the CuO-indexed peaks' intensity magnitude was highest when using 4 g of $Cu(NO_3)_2{\cdot}3H_2O$, especially (1 1 1). The ZnO-CuO NCs spectra are shown in Figure 4.

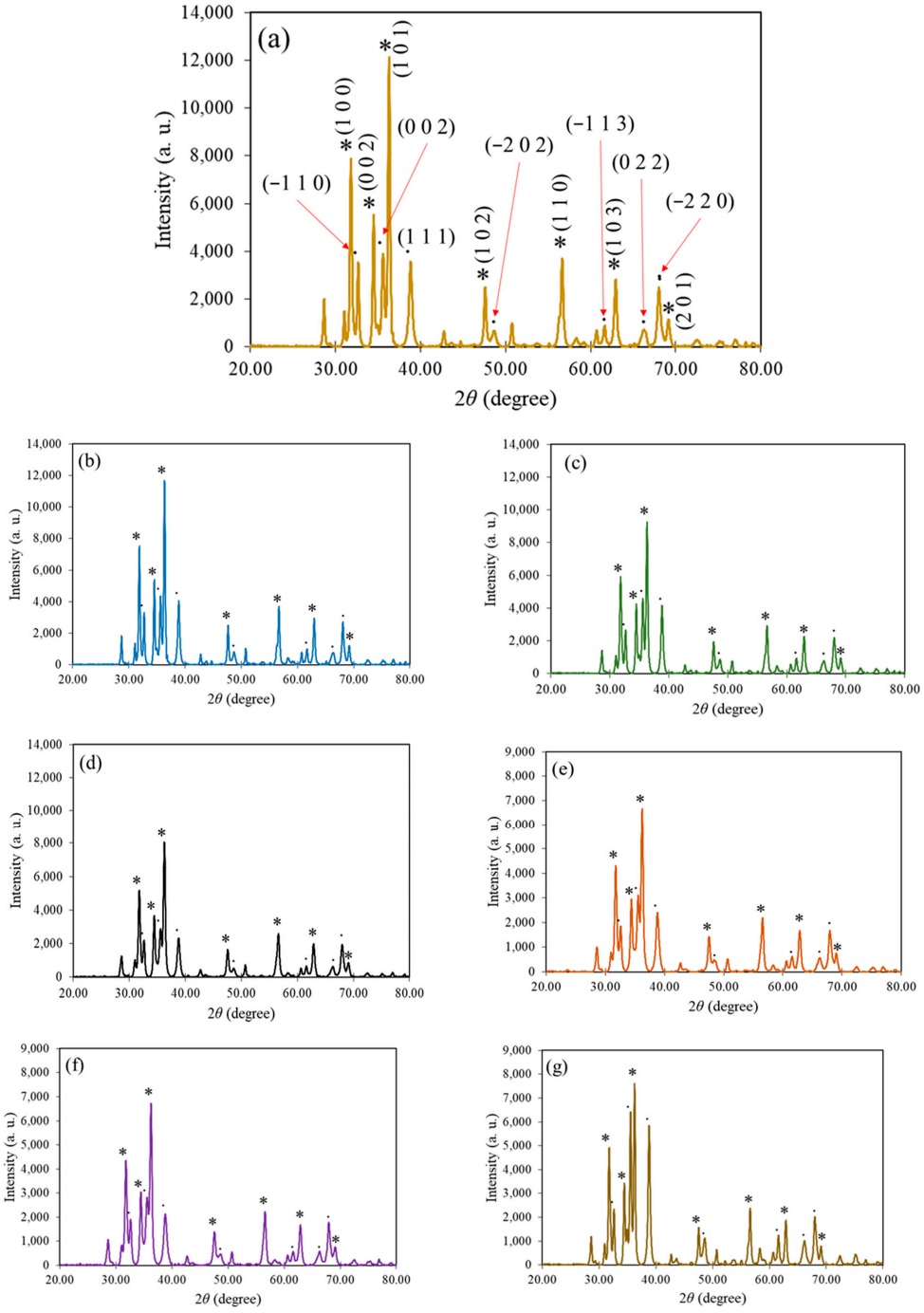

Figure 4. XRD spectra green-synthesized ZnO-CuO NCs using (**a**) 0.02 g/mL, (**b**) 0.03 g/mL, (**c**) 0.04 g/mL and (**d**) 0.05 g/mL of mangosteen leaf extract; calcinated at (**e**) 300 °C and (**f**) 400 °C, respectively, using 2 g of $Cu(NO_3)_2{\cdot}3H_2O$. Meanwhile, (**g**) is the XRD spectrum of 4 g of $Cu(NO_3)_2{\cdot}3H_2O$ calcinated at 500 °C using 0.05 g/mL of mangosteen leaf aqueous extract. All the lattice faces are represented in (**a**). Note that "*" represents ZnO, while "·" represents CuO.

The crystallinity of green-synthesized ZnO-CuO NCs was significantly affected by the mangosteen leaf aqueous concentration compared to calcination temperature and added $Cu(NO_3)_2{\cdot}3H_2O$ weight (Table 3). As shown in Equation (2), Debye–Scherrer's formula was used to calculate the crystalline size of ZnO-CuO NCs [35].

$$D = \frac{0.94\lambda}{\beta cos\theta} \quad (2)$$

where D is the crystalline size of NPs, λ is the X-ray wavelength, β is the full-width half-maximum (FWHM) of the peak and θ is the Bragg angle. In general, the crystalline size of the ZnO-CuO NCs was in the range of 18.17 to 28.51 nm. The decrement in crystalline size of ZnO-CuO NCs at elevated mangosteen leaf aqueous extract concentrations (from 28.51 nm to 18.17 nm) and calcination temperature (from 22.25 nm to 18.17 nm) was obtained. In contrast, a slight increment in the crystalline size of ZnO-CuO NCs, from 18.17 nm to 22.29 nm, when the weight of the added $Cu(NO_3)_2{\cdot}3H_2O$ increased from 2 g to 4 g.

Table 3. Crystalline sizes, dislocation density and micro strain of green-synthesized ZnO-CuO NCs at different parameters of synthesizing conditions.

Mangosteen Leaf Aqueous Extract Concentration (g/mL)	Calcination Temperature (°C)	Weight of $Zn(NO_3)_2{\cdot}6H_2O$ (g)	Weight of $Cu(NO_3)_2{\cdot}3H_2O$ (g)	ZnO Crystalline Size (nm)	CuO Crystalline Size (nm)	Crystalline Size (nm)	Dislocation Density (10^{14} cm^{-1})	Micro Strain (10^{-4})
0.02	500	4.0	2.0	31.98	25.03	28.51	12.31	1.35
0.03	500	4.0	2.0	28.67	25.23	26.95	13.77	1.32
0.04	500	4.0	2.0	27.42	23.23	25.32	15.59	1.40
0.05	500	4.0	2.0	21.10	15.23	18.17	30.30	2.77
0.05	300	4.0	2.0	23.13	21.37	22.25	20.19	1.69
0.05	400	4.0	2.0	21.94	18.52	20.23	24.42	1.86
0.05	500	4.0	4.0	20.47	20.31	22.29	20.13	1.63

The ZnO-CuO NCs dislocation density was estimated using Williamson and Smallman's formula [35] in Equation (3).

$$\delta = \frac{1}{D^2} \tag{3}$$

where δ is the dislocation density of NPs and D is the NPs' crystalline size. The ZnO-CuO NCs' dislocation density was in the range of 12.31×10^{14} to 30.30×10^{14} cm^{-1}. An increment in dislocation density was obtained when higher mangosteen leaf aqueous extract concentrations (from 12.31×10^{14} cm^{-1} to 30.30×10^{14} cm^{-1}) and calcination temperatures (from 20.19×10^{14} cm^{-1} to 30.30×10^{14} cm^{-1}) were applied. However, their dislocation density decreased from 30.30×10^{14} cm^{-1} to 20.13×10^{14} when more $Cu(NO_3)_2{\cdot}3H_2O$ was added during the green synthesis of ZnO-CuO NCs.

Equation (4) was used to calculate the micro strain of the ZnO-CuO NCs [35].

$$\varepsilon = \frac{\beta cos\theta}{4} \tag{4}$$

where ε is the micro strain of NPs, β is the FWMH of the peak and θ is the Bragg angle. Greater micro strain in ZnO-CuO NCs was found at higher concentrations of mangosteen leaf aqueous extract (from 1.35×10^{-4} to 2.77×10^{-4}) and calcination temperatures (from 1.69×10^{-4} to 2.77×10^{-4}), which was contradictory to when more $Cu(NO_3)_2{\cdot}3H_2O$ was added (from 2.77×10^{-4} to 1.63×10^{-4}).

3.5. FE-SEM Spectroscopy Analysis

The particle size of ZnO-CuO NCs was in the range of 39.10 to 74.53 nm, as tabulated in Table 4. The particle size decreased at elevated mangosteen leaf aqueous extract concentrations (61.46 nm decreased to 39.10 nm) and calcination temperatures (74.53 nm decreased to 39.10 nm). In contrast, a larger particle size was found when 4 g of $Cu(NO_3)_2{\cdot}3H_2O$ (65.18 nm) was used compared to 2 g of $Cu(NO_3)_2{\cdot}3H_2O$ (39.10 nm) in green synthesizing ZnO-CuO NCs. The trends of the particle size of the biogenic ZnO-CuO NCs were in accordance with the analyzed XRD results and tabulated in Table 4. The SEM micrographs are shown in Figure 5.

Table 4. Particle sizes and morphologies of green-synthesized ZnO-CuO NCs at different synthesizing condition parameters.

Mangosteen Leaf Aqueous Extract Concentration (g/mL)	Calcination Temperature (°C)	Weight of $Zn(NO_3)_2 \cdot 6H_2O$ (g)	Weight of $Cu(NO_3)_2 \cdot 3H_2O$ (g)	Particle Size (nm)	Morphology
0.02	500	4.0	2.0	61.46	Agglomerated with irregular nanostructure
0.03	500	4.0	2.0	56.27	Agglomerated with quasi-spherical nanostructure
0.04	500	4.0	2.0	55.23	Agglomerated with lobed nanostructure
0.05	500	4.0	2.0	39.10	Agglomerated and uniformly distributed with spherical nanostructure
0.05	300	4.0	2.0	74.53	Highly agglomerated with quasi-spherical nanostructure
0.05	400	4.0	2.0	53.71	Agglomerated with spherical nanostructure
0.05	500	4.0	4.0	65.18	Agglomerated with spherical nanostructure

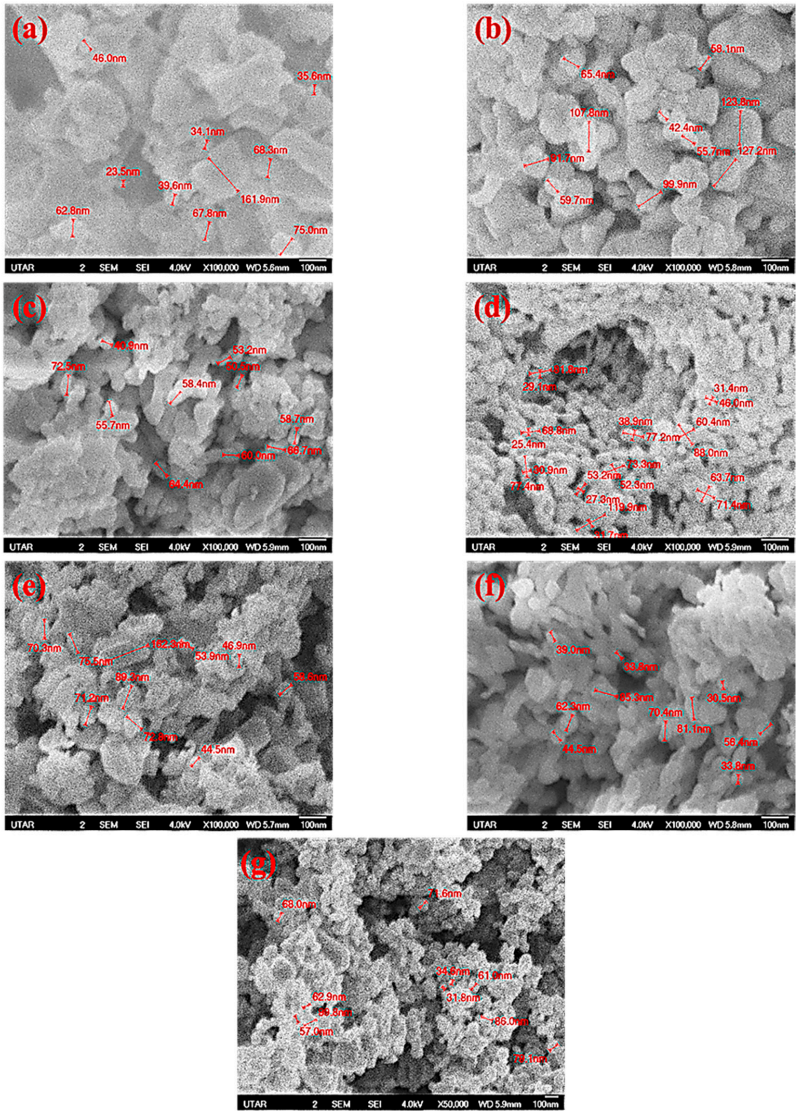

Figure 5. SEM micrographs of green-synthesized ZnO-CuO NCs using (**a**) 0.02 g/mL, (**b**) 0.03 g/mL, (**c**) 0.04 g/mL and (**d**) 0.05 g/mL of mangosteen leaf extract; calcinated at (**e**) 300 °C and (**f**) 400 °C, respectively, using 2 g of $Cu(NO_3)_2 \cdot 3H_2O$. Meanwhile, (**g**) is the SEM image of 4 g of $Cu(NO_3)_2 \cdot 3H_2O$ calcinated at 500 °C using 0.05 g/mL of mangosteen leaf aqueous extract.

3.6. EDX Spectroscopy Analysis

The copper-to-zinc atomic percentage ratio was similar to the copper precursor-to-zinc precursor weight ratio used in synthesizing ZnO-CuO NCs. Neither the mangosteen leaf aqueous extract concentration nor the calcination temperature applied significantly influenced the detected element atomic percentage, as stated in Table 5. On the other hand, compared to 2 g of $Cu(NO_3)_2 \cdot 3H_2O$, an obvious increment in copper atomic percentage (18.44%) and its intensity (around 8 keV) were observed by using 4 g of $Cu(NO_3)_2 \cdot 3H_2O$ in synthesizing ZnO-CuO NCs. The previous copper atomic percentage was only 12.55%. Overall, the synthesized ZnO-CuO NCs depicted the highest atomic percentage in oxygen (60.16–66.25%), followed by zinc atomic percentage (20.10–26.98%) and copper atomic percentage (11.64–18.44%). The presence of an oxygen peak indicated zinc and copper were in oxidized form, and no impurity was found in EDX spectra (Figure 6).

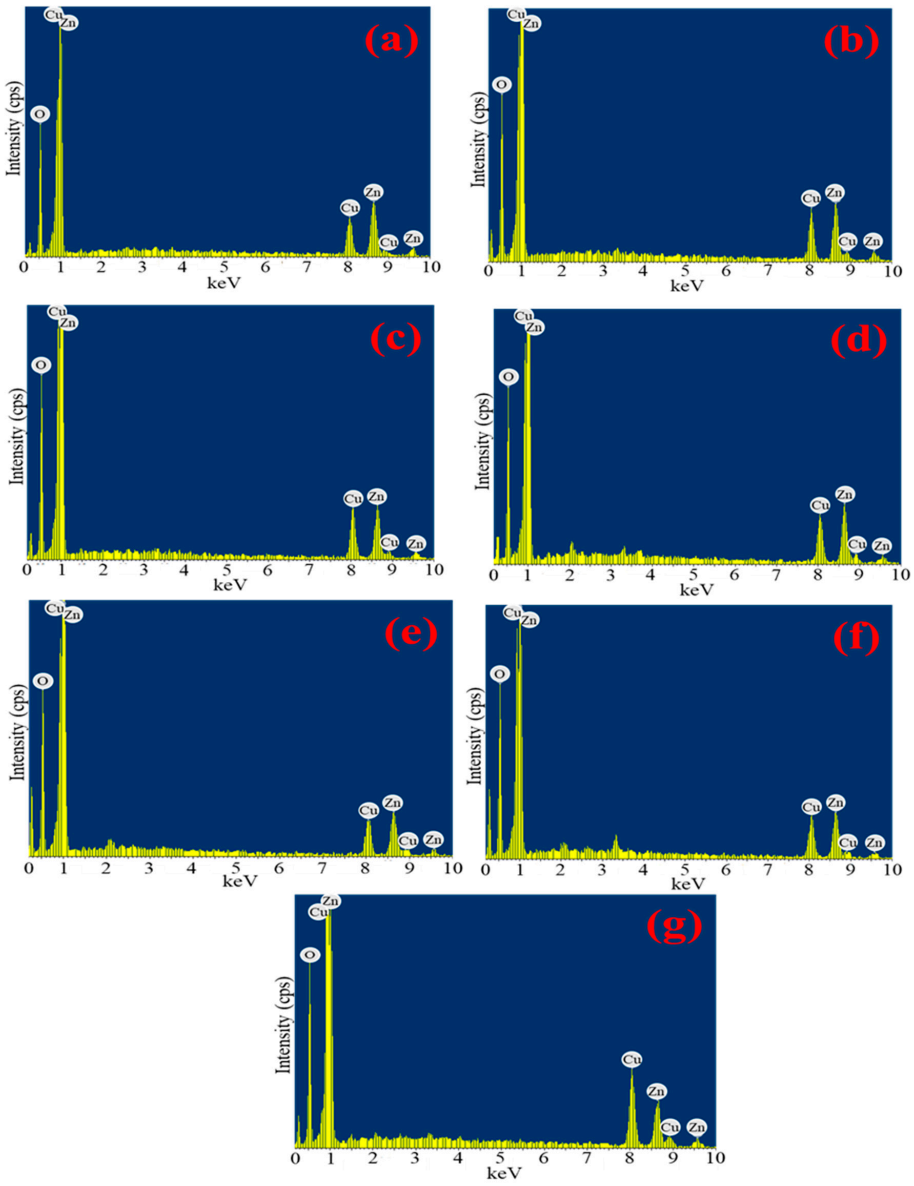

Figure 6. EDX spectra of green-synthesized ZnO-CuO NCs using (**a**) 0.02 g/mL, (**b**) 0.03 g/mL, (**c**) 0.04 g/mL and (**d**) 0.05 g/mL of mangosteen leaf extract; calcinated at (**e**) 300 °C and (**f**) 400 °C, respectively, using 2 g of $Cu(NO_3)_2 \cdot 3H_2O$ Meanwhile, (**g**) is the EDX spectrum of 4 g of $Cu(NO_3)_2 \cdot 3H_2O$ calcinated at 500 °C using 0.05 g/mL of mangosteen leaf aqueous extract.

Table 5. Atomic percentage of green-synthesized ZnO-CuO NCs at different parameters of synthesizing conditions.

Mangosteen Leaf Aqueous Extract-Concentration (g/mL)	Calcination Temperature (°C)	Weight of $Zn(NO_3)_2 \cdot 6H_2O$ (g)	Weight of $Cu(NO_3)_2 \cdot 3H_2O$ (g)	Oxygen Atomic Percentage	Copper Atomic Percentage	Zinc Atomic Percentage
0.02	500	4.0	2.0	62.28	13.03	24.68
0.03	500	4.0	2.0	60.16	12.86	26.98
0.04	500	4.0	2.0	63.25	13.10	23.65
0.05	500	4.0	2.0	62.41	12.55	25.03
0.05	300	4.0	2.0	66.25	12.28	21.47
0.05	400	4.0	2.0	66.20	11.64	22.16
0.05	500	4.0	4.0	61.45	18.44	20.10

3.7. Comparison with Other Studies

The lowest energy bandgap, and smallest crystalline and particle sizes of the mangosteen leaf aqueous extract-mediated ZnO-CuO NCs were selected to compare with other reports, as shown in Table 6. By using less $Cu(NO_3)_2 \cdot 3H_2O$, the selected ZnO-CuO NCs' energy bandgap, crystalline and particle sizes was comparable to other reports. This proved that ZnO-CuO NCs green synthesized in the current study were more cost-effective and eco-friendly when using a mangosteen leaf aqueous extract.

Table 6. Comparison of plant extract-mediated ZnO-CuO NCs with other studies.

Plant Extract	Plant Extract Concentration (g/mL)	Calcination Temperature (°C)	Zinc Salt Added (g)	Copper Salt Added (g)	Energy Bandgap (eV)	Crystalline Size (nm)	Particle Size (nm)	Reference
Theobroma cacao seed bark	0.20 [1]	400	0.03 M	0.01 M	-	10.00	20.0–50.0	[6]
D. caffra leaf	0.10	400	18.35 [2]	3.19 [3]	-	23.21	20.0–32.0	[20]
V. sinaiticum Benth	0.10	500	5.0	1.25	2.74	18.00	-	[21]
S. nigra L. shoot	0.14	400	1.6	0.8	-	-	20.0–130.0	[22]
G. mangostana L. leaf	0.05	500	4.0	2.0	2.57	18.17	25.4–60.4	Current study

[1] 0.1 mol, [2] 0.02 mol, [3] Extracted using methanol, fractional by distilled water and n-hexane.

4. Discussion

The appearance of an absorption peak at 479 cm^{-1} in mangosteen leaf aqueous extract can be attributed to the $\pi \rightarrow \pi^*$ transition [36]. On the other hand, the absorption peaks at 305 cm^{-1} and 308 cm^{-1} indicated the *d-d* transition of the $Cu(NO_3)_2 \cdot 3H_2O$ and $Zn(NO_3)_2 \cdot 6H_2O$, respectively. The presence of phytochemicals in the mangosteen leaf aqueous extract led to the occurrence of surface plasmon resonance (SPR) phenomena at a specific wavelength. The change in color of the leaf aqueous extract from light brown to brown upon the addition of the precursors revealed the reduction of zinc(II) ions to zinc(0) and copper(II) to copper(0), followed by oxidation into ZnO-CuO [17,37,38]. As a result, the absorption peaks of the ZnO-CuO NCs were red-shifted to a higher wavelength due to the formation of secondary electronic states, influenced by the metal oxide conjugation with electronic transitions between the valence band and conduction band and the exchange interaction of *s*, *p-d* spin within the atoms of metal and oxygen [23].

Regarding the energy bandgap, Ma et al. (2019) [39] reported that the copper precursor did not significantly affect it. However, Fouda et al. observed a significant decrease in the energy bandgap of ZnO-CuO NCs with an increase in the copper precursor amount [40]. Similarly, a decreasing trend in energy bandgap was observed when higher leaf aqueous extract concentrations and calcination temperatures were applied. According to the energy bandgap theory, the energy bandgap of NCs should increase or decrease due to the splitting of each level into a number of levels equal to the number of interacting atoms. In the case of hetero-structured NCs, the bands may overlap [41]. Moreover, the energy bandgap of ZnO-CuO NCs involved coupled transitions from the O_2 (*2p*) valance band to zinc(II) ($3d^1$–*4s*) and copper(II) ($3d^9$) ion conduction bands [42]. Additionally, the presence of CuO, acting as an impurity, reduces the energy bandgap in ZnO-CuO NCs [6,23], and this effect became more significant with higher concentrations of mangosteen leaf aqueous extract and higher calcination temperatures, suggesting the presence of a higher amount of CuO in ZnO-CuO NCs. Also, the redshift in the energy bandgap could be attributed to the interactions between electrons in the localized *d*-orbital of copper ions, which replaced zinc ions and the band electrons in the NCs [43]. This phenomenon makes the NCs efficient in light harvesting for photocatalytic applications [21].

The high PL indicates significant recombination of charge carriers, while low PL suggests maximum charge separation, which is beneficial for the photo-degradation of the processes [6,21,23,42]. The emission peaks of the ZnO-CuO NCs in the violet region (390–405 nm) were attributed to near-band-edge (NBE) emission caused by the defect states in ZnO and CuO [6,21,42]. Furthermore, the lower separation of charge carriers observed in ZnO-CuO NCs calcinated at high temperatures could be attributed to the reduced presence of oxygen vacancies, leading to the enhancement of NBE emission intensity [42].

The phytochemicals present in the mangosteen leaf aqueous extract, such as xanthones, flavonoids and terpene [30–33], were responsible for the observed functional groups. These compounds played a crucial role as capping, stabilizing and reducing agents during the green synthesis of ZnO-CuO NCs, primarily through electrostatic and steric stabilization mechanisms [32,44]. The vibration of the CuO and ZnO bonds was supported by previous studies [4–6,40,45,46]. The bands corresponding to metal oxides and hydroxides are typically located below 1000 cm^{-1} (fingerprint region) due to interatomic vibrations [47]. The sharp band observed in the Zn-O bond vibration confirmed the presence of a strong hexagonal-wurtzite single-phase of ZnO [18]. Additionally, the absence of Cu_2O could be inferred from the location of Cu-O bond vibration [42], as depicted in Figure 3. Furthermore, slight shifts in the bands indicated structural changes in ZnO-CuO NCs due to the incorporation of an additional element [43]. Changes in the intensity of the bands may be attributed to the variations in the interaction of functional groups from the plant extract under different controlled parameters.

The XRD patterns shown in Figure 4 confirmed the successful biosynthesis of ZnO-CuO NCs [35,40]. Previous literature reports have suggested that NCs with less than 15% of copper exhibited a one-phase wurtzite-like $Cu_xZn_{1-x}O$, while those with a higher copper content appeared as a tenorite-like oxide phase, $Zn_xCu_{1-x}O$ [20,23]. The higher peak intensity of ZnO peaks compared to CuO peaks indicate a higher percentage of ZnO in ZnO-CuO NCs [20,22]. Furthermore, the role of ZnO as a coating material led to lower peak crystallization of CuO [22]. The highest intensity at (1 0 1) corresponded to a ZnO crystal structure grown in the *a*-direction [39]. The intensity of indexed CuO peaks was highest when 4 g of $Cu(NO_3)_2{\cdot}3H_2O$ was used, indicating the contribution of copper to the formation of ZnO-CuO NCs [21,35,40], which also reflected its higher weight percentage [45,46]. The crystalline size of the ZnO-CuO NCs was similarly reported in Adeyemi et al.'s study [20]. The decrease in crystalline size of the ZnO-CuO NCs with increasing concentrations of mangosteen leaf aqueous extract and calcination temperatures demonstrated the effectiveness of phytochemicals in the plant extract for capping and stabilizing the ZnO-CuO NCs [48], particularly when a high concentration of mangosteen leaf aqueous extract and high calcination temperature were applied. In contrast, a slight increase in

the crystalline size of the ZnO-CuO NCs was observed when more $Cu(NO_3)_2 \cdot 3H_2O$ was added, indicating that the crystallinity of the synthesized NCs was greatly influenced by the variations in the precursor added [18]. However, these results differed from those reported in Fouda et al.'s study, where the crystalline size of their ZnO-CuO NCs decreased with the addition of more copper precursors during synthesis [40]. The broadening of peaks in the XRD pattern of ZnO-CuO NCs was caused by the strain resulting from non-uniform lattice distortion and crystal phase dislocation due to the mismatch in the sizes of zinc and copper atoms [35,42]. Consequently, the presence of a greater number of interfaces in each volume led to a smaller crystalline size [34], and the level of micro strain in the synthesized material increased as the size decreased [42], which was consistent with the results obtained from the calculated crystalline size.

Agglomerated spherical nanostructures were observed in mangosteen leaf aqueous extract-mediated ZnO-CuO, as depicted in Figure 5. This can be attributed to several factors, including the high viscosity of the plant extract [49], the surface physicochemical characteristics [50–53], the strong forces of attraction between particles [44,54], and the oxidation of metal oxide NPs or NCs [55]. The agglomeration of ZnO-CuO NCs was also influenced by the reduction of salt precursors to zinc and copper ion nucleation mediated by the mangosteen leaf aqueous extract, indicating their role as capping and reducing agents during the formation of ZnO-CuO NCs [43]. The formation of spherical nanostructures (0.05 g/mL) progressively occurred with increasing concentrations of mangosteen leaf aqueous extract, transitioning from irregular nanostructures at low concentrations (0.02 g/mL) of leaf aqueous extract. This may be due to greater isotropic aggregation at the isoelectric point, resulting in strong particle cohesion and the formation of nearly spherical structures [53,56,57] accompanied by the coarsening and coalescence of the NCs [9,11].

Similar results have been reported in terms of EDX analysis by Elemike et al.'s study [23]. The presence of only zinc, copper and oxygen peaks in all ZnO-CuO NCs in the EDX spectra suggests the purity of the green-synthesized ZnO-CuO NCs [20].

Although Yulizar et al.'s study [6] suggested crosslinking between zinc hydroxide and copper hydroxide in the formation of ZnO-CuO NCs, the mechanism and bonding involved in the green synthesis of ZnO-CuO NCs were not clearly addressed by researchers. Phytochemicals present in plants with functional groups, such as -C-O-C-, -C-O-, -C=C- and –C=O- in flavonoids, alkaloids, phenols and anthracenes, have been hypothesized to play a significant role in reducing, capping and stabilizing green-synthesized nanomaterials [58,59]. Xanthones, such as 1, 5, 8-trihydroxy-3-methoxy-2-(3-methylbut-2-enyl) xanthone and 1, 6-dihydroxy-3-methoxy-2-(3-methyl-2-buthenyl)-xanthone, are the major compounds in mangosteen leaf [60]. During chelation, electrons from the precursors' zinc and copper atoms were donated to form positively charged zinc(II) and copper(II) ions, respectively, which then formed metal complexes with the phytochemicals. These metal complexes subsequently bonded with negatively charged oxygen(II) ions during calcination [61]. Another possible mechanism for the formation of ZnO-CuO NCs was bio reduction, where the divalent oxidation state of zinc and copper were reduced to a zero-valent state by the phytochemicals present in the mangosteen leaf aqueous extract, as indicated by the immediate color change during the green synthesis [62]. ZnO and CuO nuclei were formed after the metallic zinc and copper reacted with the dissolved oxygen in the precursor solution [61], and coordinate covalent bonds were subsequently formed between ZnO and CuO through the lone-pair electron from the oxygen atoms of the metal oxides. A strong framework of ZnO-CuO NCs was then produced during calcination [6]. The possible mechanism and bonding in green synthesizing ZnO-CuO NCs is represented in Scheme 1.

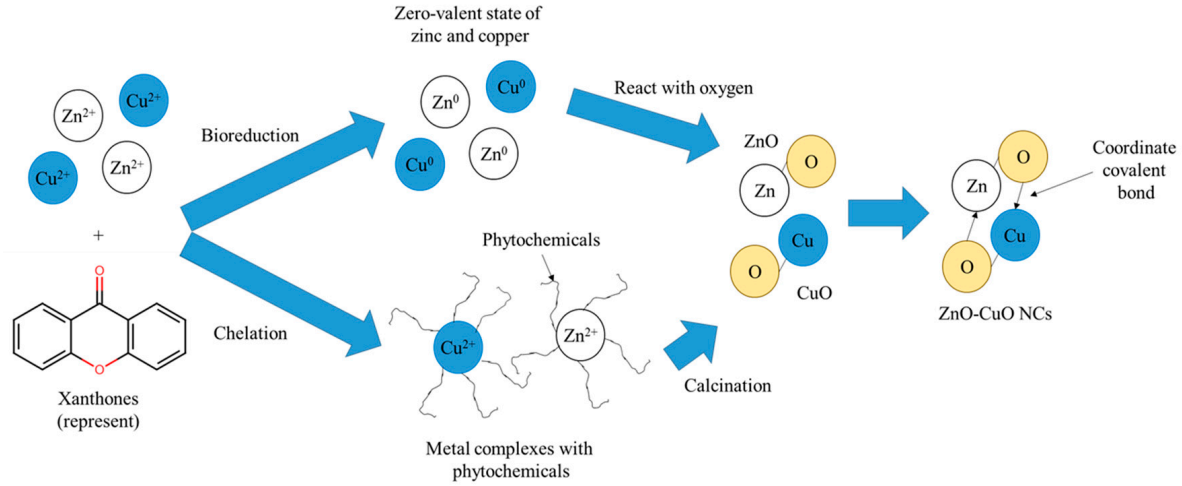

Scheme 1. Possible mechanism of green-synthesized ZnO-CuO NCs via bio reduction and chelation with the presence of phytochemicals (represented by xanthones). Coordinate covalent bond formation between ZnO and CuO by lone-pair electrons from the bonded oxygen atom was proposed to link both metal oxides in NCs.

5. Conclusions

ZnO-CuO NCs were successfully green synthesized using a mangosteen leaf aqueous extract at different concentrations (0.02, 0.03, 0.04 and 0.05 mg/mL), calcination temperatures (300, 400 and 500 °C) and weights of $Cu(NO_3)_2 \cdot 3H_2O$ (2 and 4 g). The properties of ZnO-CuO NCs were significantly influenced by the green synthesis parameters, including the concentration of the plant extract, calcination temperature and precursor weight. The energy bandgap and crystalline properties of the ZnO-CuO NCs were notably affected by the concentration of the mangosteen leaf aqueous extract and the calcination temperature. However, the intensity of the PL spectrum was solely dependent on the applied calcination temperature. Moreover, the atomic percentage of copper-to-zinc was primarily affected by the weight of the zinc and copper precursor used to synthesize ZnO-CuO NCs. The particle size and morphology were significantly influenced by varied parameters employed in the green synthesis of ZnO-CuO NCs. However, the locations of the FTIR bands in the ZnO-CuO NCs remained consistent throughout the study. The presence of coordinate covalent bonds between ZnO and CuO facilitated by the lone pair of electrons from the oxygen atoms was suggested. The study clearly illustrated the effects of plant extract concentrations, calcination temperatures and precursor amount on the optical, structural and morphological properties during the green synthesis of ZnO-CuO NCs. These findings provide valuable insights for researchers to synthesize ZnO-CuO NCs with specific properties for future applications.

Author Contributions: Conceptualization, M.A. (Mohammod Aminuzzaman), L.-H.T. and M.A. (Md. Akhtaruzzaman); methodology, M.A. (Mohammod Aminuzzaman); validation, Y.F.W.; formal analysis, Y.B.C., M.A. (Mohammod Aminuzzaman) and A.W.; investigation, Y.B.C. and S.D.; resources, Y.B.C.; data curation, Y.B.C.; writing—original draft preparation, Y.B.C.; writing—review and editing, M.A. (Mohammod Aminuzzaman), L.-H.T. and Y.F.W..; visualization, Y.B.C.; supervision, M.A. (Mohammod Aminuzzaman), L.-H.T. and M.A. (Md. Akhtaruzzaman); project administration, M.A. (Mohammod Aminuzzaman) and L.-H.T.; funding acquisition, M.A. (Mohammod Aminuzzaman) and L.-H.T. All authors have read and agreed to the published version of the manuscript.

Funding: This research was funded by the Universiti Tunku Abdul Rahman (UTAR) through UTARRF (IPSR/RMC/UTARRF202-C2/M01).

Institutional Review Board Statement: Not applicable.

Informed Consent Statement: Not applicable.

Data Availability Statement: The data presented in this study are available upon request from the corresponding author.

Acknowledgments: The authors extended our appreciation to the Universiti Tunku Abdul Rahman (UTAR) for providing financial support through UTARRF (IPSR/RMC/UTARRF/202-C2/M01) and research facilities to carry out the research work. Authors also extended their appreciation to Wong Ling Shing in giving advices and suggestions in improving the English fluency of the manuscript.

Conflicts of Interest: The authors declare no conflict of interest.

References

1. Das, S.; Srivastava, V.C. An overview of the synthesis of CuO-ZnO nanocomposite for environmental and other applications. *Nanotechnol. Rev.* **2018**, *7*, 267–282. [CrossRef]
2. Khan, S.A.; Noreen, F.; Kanwal, S.; Iqbal, A.; Hussain, G. Green synthesis of ZnO and Cu-doped ZnO nanoparticles from leaf extracts of *Abutilon indicum*, *Clerodendrum infortunatum*, *Clerodendrum inerme* and investigation of their biological and photocatalytic activities. *Mater. Sci. Eng. C* **2017**, *82*, 46–59. [CrossRef] [PubMed]
3. Vibitha, B.V.; Anitha, B.; Tharayil, N.J. Green synthesis of ZnO:CuO nanocomposites by *Aloe barbadansis* leaf extract: Structure and photo catalytic properties. In Proceedings of the AIP Conference Proceedings, International Conference on Energy and Environment 2019, Guimaraes, Portugal, 16–17 May 2019.
4. Rajith Kumar, C.R.; Betageri, V.S.; Nagaraju, G.; Pujar, G.H.; Onkarappa, H.S.; Latha, M.S. One-pot green synthesis of ZnO-CuO nanocomposite and their enhanced photocatalytic and antibacterial activity. *Adv. Nat. Sci. Nanosci. Nanotechnol.* **2020**, *11*, 015009. [CrossRef]
5. Sakib, A.A.M.; Masum, S.M.; Hoinkis, J.; Islam, R.; Molla, M.A.I. Synthesis of CuO/ZnO nanocomposites and their application in photodegradation of toxic textile dye. *J. Compos. Sci.* **2019**, *3*, 91–103. [CrossRef]
6. Yulizar, Y.; Bakri, R.; Apriandanu, D.O.B.; Hidayat, T. ZnO/CuO nanocomposite prepared in one-pot green synthesis using seed bark extract of *Theobroma cacao*. *Nano-Struct. Nano-Objects* **2018**, *16*, 300–305. [CrossRef]
7. Bano, S.; Pillai, S. Green synthesis of calcium oxide nanoparticles at different calcination temperatures. *World J. Sci. Technol. Sustain. Dev.* **2020**, *17*, 283–295. [CrossRef]
8. Hassan, S.E.-D.; Fouda, A.; Saied, E.; Farag, M.M.S.; Eid, A.M.; Barghoth, M.G.; Awad, M.A.; Hamza, M.F.; Awad, M.F. *Rhizopus oryzae*-mediated green synthesis of magnesium oxide nanoparticles (MgO-NPs): A promising tool for antimicrobial, mosquitocidal action, and tanning effluent treatment. *J. Fungi* **2021**, *7*, 372–396. [CrossRef]
9. Jameel, M.S.; Aziz, A.A.; Dheyab, M.A. Green synthesis: Proposed mechanism and factors influencing the synthesis of platinum nanoparticles. *Green. Process Synth.* **2020**, *9*, 386–398. [CrossRef]
10. Khan, A.; Shabir, D.; Ahmad, P.; Khandaker, M.U.; Faruque, M.R.; Din, I.U. Biosynthesis and antibacterial activity of MgO-NPs produced from *Camellia-sinensis* leaves extract. *Mater. Res. Express* **2021**, *8*, 015402. [CrossRef]
11. Mazli, S.R.A.; Yusoff, H.M.; Idris, N.H. Synthesis of zinc oxide nanoparticles by using *Aloe vera* leaf extract as pontential anode material in lithium ion battery. *Univ. Malaysia Teren. J. Undergrad. Res.* **2020**, *2*, 1–8.
12. Xu, J.; Huang, Y.; Zhu, S.; Abbes, N.; Jing, X.; Zhang, L. A review of the green synthesis of ZnO nanoparticles using plant extracts and their prospects for application in antibacterial textiles. *J. Eng. Fiber Fabr.* **2021**, *16*, 1–14. [CrossRef]
13. Efenberger-Szmechtyk, M.; Nowak, A.; Czyzowska, A. Plant extracts rich in polyphenols: Antibacterial agents and natural preservatives for meat and meat products. *Crit. Rev. Food Sci. Nutr.* **2020**, *61*, 149–178. [CrossRef]
14. Prasanth, R.; Dinesh Kumar, S.; Jayalakshmi, A.; Singaravelu, G.; Govindaraju, K.; Ganesh Kumar, V. Green synthesis of magnesium oxide nanoparticles and their antibacterial activity. *Indian. J. Geo Mar. Sci.* **2019**, *48*, 1210–1215.
15. Shammout, M.W.; Awwad, A.M. A novel route for the synthesis of copper oxide nanoparticles using *Bougainvillea* plant flowers extract and antifungal activity evaluation. *Int. Sci. Organ.* **2021**, *7*, 71–78.
16. Kumar, H.; Bhardwaj, K.; Dhanjal, D.S.; Nepovimova, E.; Şen, F.; Regassa, H.; Singh, R.; Verma, R.; Kumar, V.; Kumar, D.; et al. Fruit extract mediated green synthesis of metallic nanoparticles: A new avenue in pomology applications. *Int. J. Mol. Sci.* **2020**, *21*, 8458. [CrossRef] [PubMed]
17. Kureshi, A.A.; Vaghela, H.M.; Kumar, S.; Singh, R.; Kumari, P. Green synthesis of gold nanoparticles mediated by *Garcinia* fruits and their biological applications. *Pharm. Sci.* **2021**, *27*, 238–250. [CrossRef]
18. Kaningini, A.G.; Azizi, S.; Sintwa, N.; Mokalane, K.; Mohale, K.C.; Mudau, F.N.; Maaza, M. Effect of optimized precursor concentration, temperature, and doping on optical properties of ZnO nanoparticles synthesized via a green route using bush tea (*Athrixia phylicoides* DC.) leaf extracts. *ACS Omega* **2022**, *7*, 31658–31666. [CrossRef] [PubMed]
19. Kumar, I.; Mondal, M.; Sakthivel, N. Green synthesis of phytogenic nanoparticles. In *Green Synthesis, Characterization and Applications of Nanoparticles*; Shukla, A.K., Iravani, S., Eds.; Elsevier Inc.: Amsterdam, The Netherlands, 2019; pp. 37–73.
20. Adeyemi, J.O.; Onwudiwe, D.C.; Oyedeji, A.O. Biogenic synthesis of CuO, ZnO, and CuO–ZnO nanoparticles using leaf extracts of *Dovyalis caffra* and their biological properties. *Molecules* **2022**, *27*, 3206. [CrossRef]
21. Bekru, A.G.; Tufa, L.T.; Zelekew, O.A.; Goddati, M.; Lee, J.; Sabir, F.K. Green synthesis of a CuO–ZnO nanocomposite for efficient photodegradation of methylene blue and reduction of 4-nitrophenol. *ACS Omega* **2022**, *7*, 30908–30919. [CrossRef]

22. Cao, Y.; Dhahad, H.A.; El-Shorbagy, M.A.; Alijani, H.Q.; Zakeri, M.; Heydari, A.; Bahonar, E.; Slouf, M.; Khatami, M.; Naderifar, M.; et al. Green synthesis of bimetallic ZnO–CuO nanoparticles and their cytotoxicity properties. *Sci. Rep.* **2021**, *11*, 23479. [CrossRef]
23. Elemike, E.E.; Onwudiwe, D.C.; Singh, M. Eco-friendly synthesis of copper oxide, zinc oxide and copper oxide–zinc oxide nanocomposites, and their anticancer applications. *J. Inorg. Organomet. Polym. Mater.* **2019**, *30*, 400–409. [CrossRef]
24. Govindasamy, G.A.; Mydin, R.B.S.M.N.; Harun, N.H.; Sreekantan, S. Calcination temperatures, compositions and antimicrobial properties of heterostructural ZnO–CuO nanocomposites from *Calotropis gigantea* targeted for skin ulcer pathogens. *Sci. Rep.* **2020**, *11*, 99. [CrossRef] [PubMed]
25. Hiew, C.W.; Lee, L.J.; Junus, S.; Tan, Y.N.; Chai, T.T.; Ee, K.Y. Optimization of microwave-assisted extraction and the effect of microencapsulation on mangosteen (*Garcinia mangostana* L.) rind extract. *Food Sci. Technol.* **2021**, *42*, e35521. [CrossRef]
26. Huang, X.; Zhou, X.; Dai, Q.; Qin, Z. Antibacterial, antioxidation, UV-blocking, and biodegradable soy protein isolate food packaging film with mangosteen peel extract and ZnO nanoparticles. *Nanomaterials* **2021**, *11*, 3337. [CrossRef]
27. Mohd Basri, M.S.; Ren, B.L.M.; Talib, R.A.; Zakaria, R.; Kamarudin, S.H. Novel mangosteen-leaves-based marker ink color lightness, viscosity, optimized composition, and microstructural analysis. *Polymers* **2021**, *13*, 1581. [CrossRef]
28. Mulyono, D.; Irawati, Y.; Syah, M.J.A. Identification morphological variability of six mangosteen (*Garcinia mangostana* L.) as a conservation strategy for local varieties. *IOP Conf. Ser. Earth Environ. Sci.* **2021**, *739*, 012076. [CrossRef]
29. Syahputra, M.R.; Setiado, H.; Siregar, L.A.M.; Damanik, R.I. Morphological characteristics of mangosteen plants (*Garcinia mangostana* L.) in Langkat District, North Sumatera, Indonesia. *IOP Conf. Ser. Earth Environ. Sci.* **2021**, *782*, 042056. [CrossRef]
30. Andani, R.; Fajrina, A.; Asra, R.; Eriadi, A. Antibacterial activity test of mangosteen plants (*Garcinia mangostana* L.): A review. *Asian J. Pharm. Res. Dev.* **2021**, *9*, 164–171. [CrossRef]
31. Anggraeni, R.S. Antibacterial (*Staphylococcus aureus* and *Escherichia coli*) and Antifungal (*Saccharomyces cerevisiae*) activity assay on nanoemulsion formulation of ethanol extract of mangosteen leaves (*Garcinia mangostana* L). *J. Food Pharm. Sci.* **2021**, *9*, 351–365.
32. Jassim, A.M.N.; Shafy, G.M.; Mohammed, M.T.; Farhan, S.A.; Noori, O.M. Antioxidant, anti-inflammatory and wound healing of biosynthetic gold nanoparticles using mangosteen (*G. mangostona*). *Iraqi J. Ind. Res.* **2021**, *8*, 59–74. [CrossRef]
33. Tran, V.A.; Thi Vo, T.-T.; Thi Nguyen, M.-N.; Duy, N.D.; Doan, V.-D.; Nguyen, T.-Q.; Vu, Q.H.; Le, V.T.; Tong, T.D. Novel α-mangostin derivatives from mangosteen (*Garcinia mangostana* L.) peel extract with antioxidant and anticancer potential. *J. Chem.* **2021**, *2021*, 9985604. [CrossRef]
34. Chan, Y.B.; Selvanathan, V.; Tey, L.-H.; Akhtaruzzaman, M.; Anur, F.H.; Djearamane, S.; Watanabe, A.; Aminuzzaman, M. Effect of calcination temperature on structural, morphological and optical properties of copper oxide nanostructures derived from *Garcinia mangostana* L. leaf extract. *Nanometerials* **2022**, *12*, 3589. [CrossRef] [PubMed]
35. Hitkari, G.; Chowdhary, P.; Kumar, V.; Singh, S.; Motghare, A. Potential of copper-zinc oxide nanocomposite for photocatalytic degradation of congo red dye. *Clean. Chem. Eng.* **2022**, *1*, 100003–100009. [CrossRef]
36. Rajendran, N.K.; George, B.P.; Houreld, N.N.; Abrahamse, H. Synthesis of zinc oxide nanoparticles using *Rubus fairholmianus* root extract and their activity against pathogenic bacteria. *Molecules* **2021**, *26*, 3029. [CrossRef]
37. Sivakavinesan, M.; Vanaja, M.; Annadurai, G. Dyeing of cotton fabric materials with biogenic gold nanoparticles. *Sci. Rep.* **2021**, *1*, 13249. [CrossRef] [PubMed]
38. Trang, N.L.N.; Hoang, V.T.; Dinh, N.X.; Tam, L.T.; Le, V.P.; Linh, D.T.; Cuong, D.M.; Khi, N.T.; Anh, N.H.; Nhung, P.T.; et al. Novel eco-friendly synthesis of biosilver nanoparticles as a colorimetric probe for highly selective detection of Fe (III) ions in aqueous solution. *J. Nanomater.* **2021**, *2021*, 5527519. [CrossRef]
39. Mansoor Al-Saeedi, A.M.; Mohamad, F.K.; Ridha, N.J. Synthesis and characterization CuO-ZnO binary nanoparticles. *J. Nanostructures* **2022**, *12*, 86–96.
40. Fouda, A.; Salem, S.S.; Wassel, A.R.; Hamza, M.F.; Shaheen, T.I. Optimization of green biosynthesized visible light active CuO/ZnO nano-photocatalysts for the degradation of organic methylene blue dye. *Heliyon* **2020**, *6*, e04896–e04908. [CrossRef]
41. Rao, G.T.; Ravikumar, R.V.S.S.N. Novel Fe-doped ZnO-CdS nanocomposite with enhanced visible light-driven photocatalytic performance. *Mater. Res. Innov.* **2020**, *25*, 215–220. [CrossRef]
42. Siddiqui, V.U.; Ansari, A.; Ansari, M.T.; Akram, M.K.; Siddiqi, W.A.; Alosaimi, A.M.; Hussein, M.A.; Rafatullah, M. Optimization of facile synthesized ZnO/CuO nanophotocatalyst for organic dye degradation by visible light irradiation using response surface methodology. *Catalysts* **2021**, *11*, 1509. [CrossRef]
43. Khan, M.I.; Fatima, N.; Shakil, M.; Tahir, M.B.; Riaz, K.N.; Rafique, M.; Iqbal, T.; Mahmood, K. Investigation of in-vitro antibacterial and seed germination properties of green synthesized pure and nickel doped ZnO nanoparticles. *Phys. B Phys. Condens. Matter.* **2021**, *601*, 412563. [CrossRef]
44. Yusefi, M.; Shameli, K.; Yee, O.S.; Teow, S.Y.; Hedayatnasab, Z.; Jahangirian, H.; Webster, T.J.; Kuca, K. Green synthesis of Fe_3O_4 nanoparticles stabilized by a garcinia mangostana fruit peel extract for hyperthermia and anticancer activities. *Int. J. Nanomed.* **2021**, *16*, 2515–2532. [CrossRef] [PubMed]
45. Mohammadi-Aloucheh, R.; Habibi-Yangjeh, A.; Bayrami, A.; Latifi-Navid, S.; Asadi, A. Enhanced anti-bacterial activities of ZnO nanoparticles and ZnO/CuO nanocomposites synthesized using *Vaccinium arctostaphylos* L. fruit extract. *Artif. Cells Nanomed. Biotechnol.* **2018**, *46*, 1200–1209. [CrossRef] [PubMed]

46. Mohammadi-Aloucheh, R.; Habibi-Yangjeh, A.; Bayrami, A.; Latifi-Navid, S.; Asadi, A. Green synthesis of ZnO and ZnO/CuO nanocomposites in *Mentha longifolia* leaf extract: Characterization and their application as anti-bacterial agents. *J. Mater. Sci. Mater. Electron.* **2018**, *29*, 13596–13605. [CrossRef]
47. Haneefa, M.M.; Jayandran, M.; Balasubramanian, V. Green synthesis characterization and antimicrobial activity evaluation of manganese oxide nanoparticles and comparative studies with salicylalchitosan functionalized nanoform. *Asian J. Pharm.* **2017**, *11*, 65–74.
48. Demissie, M.G.; Sabir, F.K.; Edossa, G.D.; Gonfa, B.A. Synthesis of zinc oxide nanoparticles using leaf extract of *Lippia adoensis* (Koseret) and evaluation of its antibacterial activity. *J. Chem.* **2020**, *2020*, 7459042. [CrossRef]
49. Siddiqui, V.U.; Ansari, A.; Chauhan, R.; Siddiqi, W.A. Green synthesis of copper oxide (CuO) nanoparticles by *Punica granatum* peel extract. *Mater. Today Proc.* **2021**, *36*, 751–755. [CrossRef]
50. Phang, Y.-K.; Aminuzzaman, M.; Akhtaruzzaman, M.; Muhammad, G.; Ogawa, S.; Watanabe, A.; Tey, L.-H. Green synthesis and characterization of CuO nanoparticles derived from papaya peel extract for the photocatalytic degradation of palm oil mill effluent (POME). *Sustainability* **2021**, *13*, 796. [CrossRef]
51. Sajjad, A.; Bhatti, S.H.; Ali, Z.; Jaffari, G.H.; Khan, N.A.; Rizvi, Z.F.; Zia, M. Photoinduced fabrication of zinc oxide nanoparticles: Transformation of morphological and biological response on light irradiance. *ACS Omega* **2021**, *6*, 11783–11793. [CrossRef] [PubMed]
52. Sharma, S.; Yadav, D.K.; Chawla, K.; Lai, N.; Lai, C. Synthesis and characterization of CuO nanoparticles by *Aloe barbadensis* leaves. *Quantum J. Eng. Sci. Technol.* **2021**, *2*, 1–9.
53. You, W.; Ahn, J.C.; Boopathi, V.; Arunkumar, L.; Rupa, E.J.; Akter, R.; Kong, B.M.; Lee, G.S.; Yang, D.C.; Kang, S.C.; et al. Enhanced antiobesity efficacy of tryptophan using the nanoformulation of *Dendropanax morbifera* extract mediated with ZnO nanoparticle. *Materials* **2021**, *14*, 824. [CrossRef] [PubMed]
54. Aminuzzaman, M.; Chong, C.-Y.; Goh, W.S.; Phang, Y.-K.; Tey, L.-H.; Chee, S.-Y.; Akhtaruzzaman, M.; Ogawa, S.; Watanabe, A. Biosynthesis of NiO nanoparticles using soursop (*Annona muricata* L.) fruit peel green waste and their photocatalytic performance on crystal violet dye. *J. Clust. Sci.* **2021**, *32*, 949–958. [CrossRef]
55. Ramzan, M.; Obodo, R.M.; Mukhtar, S.; Ilyas, S.Z.; Aziz, F.; Thovhogi, N. Green synthesis of copper oxide nanoparticles using *Cedrus deodara* aqueous extract for antibacterial activity. *Mater. Today Proc.* **2021**, *36*, 576–581. [CrossRef]
56. Baharudin, K.B.; Abdullah, N.; Derawi, D. Effect of calcination temperature on the physicochemical properties of zinc oxide nanoparticles synthesized by coprecipitation. *Mater. Res. Express* **2018**, *5*, 125018. [CrossRef]
57. Naseer, M.; Aslam, U.; Khalid, B.; Chen, B. Green route to synthesize zinc oxide nanoparticles using leaf extracts of *Cassia fistula* and *Melia azadarach* and their antibacterial potential. *Sci. Rep.* **2020**, *10*, 9055. [CrossRef]
58. Jeevanandam, J.; Chan, Y.S.; Danquah, M.K. Biosynthesis of metal and metal oxide nanoparticles. *ChemBioEng Rev.* **2016**, *3*, 55–67. [CrossRef]
59. Singh, J.; Dutta, T.; Kim, K.H.; Rawat, M.; Samddar, P.; Kumar, P. "Green" synthesis of metals and their oxide nanoparticles: Applications for environmental remediation. *J. Nanobiotechnol.* **2018**, *16*, 84. [CrossRef]
60. Obolskiy, D.; Pischel, I.; Siriwatanametanon, N.; Heinrich, M. *Garcinia mangostana* L.: A phytochemical and pharmacological review. *Phyther Res.* **2009**, *23*, 1047–1065. [CrossRef]
61. Selvanathan, V.; Aminuzzaman, M.; Tan, L.X.; Yip, F.W.; Eddy Cheah, S.G.; Heng, M.H.; Tey, L.-H.; Arullappan, S.; Algethami, N.; Alharthi, S.S.; et al. Synthesis, characterization, and preliminary in vitro antibacterial evaluation of ZnO nanoparticles derived from soursop (*Annona muricata* L.) leaf extract as a green reducing agent. *J. Mater. Res. Technol.* **2022**, *20*, 2931–2941. [CrossRef]
62. Fawcett, D.; Verduin, J.J.; Shah, M.; Sharma, S.B.; Poinern, G.E.J. A review of current research into the biogenic synthesis of metal and metal oxide nanoparticles via marine algae and seagrasses. *J. Nanosci.* **2017**, *2017*, 8013850. [CrossRef]

Disclaimer/Publisher's Note: The statements, opinions and data contained in all publications are solely those of the individual author(s) and contributor(s) and not of MDPI and/or the editor(s). MDPI and/or the editor(s) disclaim responsibility for any injury to people or property resulting from any ideas, methods, instructions or products referred to in the content.